Contents lists available at ScienceDirect

Nuclear Inst. and Methods in Physics Research, A

journal homepage: www.elsevier.com/locate/nima



Exclusive J/ψ detection and physics with ECCE



S. Sirca ⁷¹, D. Sharma ¹⁸, Z. Shi ³¹, T.-A. Shibata ³⁹, C.-W. Shih ³⁸, S. Shimizu ⁵¹, U. Shrestha ⁶⁵, K. Slifer 72, K. Smith 31, D. Sokhan 19,24, R. Soltz 33, W. Sondheim 31, J. Song 11, J. Song 49,

E-mail addresses: xinbai@mail.ustc.edu.cn (X. Li), first@ustc.edu.cn (W. Zha).



^{*} Corresponding author.

```
I.I. Strakovsky <sup>21</sup>, P. Steinberg <sup>6</sup>, P. Stepanov <sup>14</sup>, J. Stevens <sup>84</sup>, J. Strube <sup>48</sup>, P. Sun <sup>11</sup>, X. Sun <sup>9</sup>,
K. Suresh<sup>74</sup>, V. Tadevosyan<sup>2</sup>, W.-C. Tang<sup>38</sup>, S. Tapia Araya<sup>26</sup>, S. Tarafdar<sup>80</sup>, L. Teodorescu<sup>7</sup>, D. Thomas<sup>77</sup>, A. Timmins<sup>67</sup>, L. Tomasek<sup>15</sup>, N. Trotta<sup>65</sup>, R. Trotta<sup>14</sup>, T.S. Tveter<sup>73</sup>, E. Umaka<sup>26</sup>,
A. Usman <sup>74</sup>, H.W. van Hecke <sup>31</sup>, C. Van Hulse <sup>23</sup>, J. Velkovska <sup>80</sup>, E. Voutier <sup>23</sup>, P.K. Wang <sup>23</sup>,
Q. Wang <sup>69</sup>, Y. Wang <sup>9</sup>, Y. Wang <sup>62</sup>, D.P. Watts <sup>88</sup>, N. Wickramaarachchi <sup>14</sup>, L. Weinstein <sup>45</sup>,
M. Williams <sup>35</sup>, C.-P. Wong <sup>31</sup>, L. Wood <sup>48</sup>, M.H. Wood <sup>8</sup>, C. Woody <sup>6</sup>, B. Wyslouch <sup>35</sup>, Z. Xiao <sup>62</sup>,
Y. Yamazaki <sup>29</sup>, Y. Yang <sup>37</sup>, Z. Ye <sup>62</sup>, H.D. Yoo <sup>87</sup>, M. Yurov <sup>31</sup>, N. Zachariou <sup>88</sup>, W.A. Zajc <sup>13</sup>,
W. Zha<sup>1,*</sup>, J.-L. Zhang<sup>56</sup>, J.-X. Zhang<sup>79</sup>, Y. Zhang<sup>62</sup>, Y.-X. Zhao<sup>25</sup>, X. Zheng<sup>79</sup>, P. Zhuang<sup>62</sup>
<sup>1</sup> University of Science and Technology of China, Hefei, China
<sup>2</sup> A. Alikhanyan National Laboratory, Yerevan, Armenia
<sup>3</sup> Institute of Physics, Academia Sinica, Taipei, Taiwan
<sup>4</sup> Augustana University, Sioux Falls, SD, USA
<sup>5</sup> Ben-Gurion University of the Negev, Beer-Sheva, Israel
<sup>6</sup> Brookhaven National Laboratory, Upton, NY, USA
<sup>7</sup> Brunel University London, Uxbridge, UK
8 Canisius College, Buffalo, NY, USA
<sup>9</sup> Central China Normal University, Wuhan, China
10 Charles University, Prague, Czech Republic
11 China Institute of Atomic Energy, Fangshan, Beijing, China
<sup>12</sup> Christopher Newport University, Newport News, VA, USA
13 Columbia University, New York, NY, USA
14 Catholic University of America, Washington DC, USA
<sup>15</sup> Czech Technical University, Prague, Czech Republic
16 Duquesne University, Pittsburgh, PA, USA
<sup>17</sup> Florida International University, Miami, FL, USA
18 Georgia State University, Atlanta, GA, USA
<sup>19</sup> University of Glasgow, Glasgow, UK
<sup>20</sup> GSI Helmholtzzentrum fuer Schwerionenforschung GmbH, Darmstadt, Germany
<sup>21</sup> The George Washington University, Washington, DC, USA
<sup>22</sup> Hebrew University, Jerusalem, Israel
<sup>23</sup> Universite Paris-Saclay, CNRS/IN2P3, IJCLab, Orsay, France
<sup>24</sup> IRFU, CEA, Universite Paris-Saclay, Gif-sur-Yvette, France
<sup>25</sup> Chinese Academy of Sciences, Lanzhou, China
<sup>26</sup> Iowa State University, Iowa City, IA, USA
<sup>27</sup> Jazan University, Jazan, Saudi Arabia
<sup>28</sup> Thomas Jefferson National Accelerator Facility, Newport News, VA, USA
<sup>29</sup> Kobe University, Kobe, Japan
30 Kyungpook National University, Daegu, Republic of Korea
31 Los Alamos National Laboratory, Los Alamos, NM, USA
32 Lehigh University, Bethlehem, PA, USA
33 Lawrence Livermore National Laboratory, Livermore, CA, USA
34 Morehead State University, Morehead, KY, USA
35 Massachusetts Institute of Technology, Cambridge, MA, USA
<sup>36</sup> Mississippi State University, Mississippi State, MS, USA
37 National Cheng Kung University, Tainan, Taiwan
38 National Central University, Chungli, Taiwan
<sup>39</sup> Nihon University, Tokyo, Japan
40 New Mexico State University, Las Cruces, NM, USA
<sup>41</sup> National Research Nuclear University MEPhI, Moscow, Russian Federation
42 Nuclear Research Center - Negev, Beer-Sheva, Israel
<sup>43</sup> National Tsing Hua University, Hsinchu, Taiwan
<sup>44</sup> National Taiwan University, Taipei, Taiwan
<sup>45</sup> Old Dominion University, Norfolk, VA, USA
<sup>46</sup> Ohio University, Athens, OH, USA
47 Oak Ridge National Laboratory, Oak Ridge, TN, USA
48 Pacific Northwest National Laboratory, Richland, WA, USA
<sup>49</sup> Pusan National University, Busan, Republic of Korea
<sup>50</sup> Rice University, Houston, TX, USA
51 RIKEN Nishina Center, Wako, Saitama, Japan
52 The State University of New Jersey, Piscataway, NJ, USA
<sup>53</sup> Center for Frontiers in Nuclear Science, Stony Brook, NY, USA
54 Stony Brook University, Stony Brook, NY, USA
55 RIKEN BNL Research Center, Upton, NY, USA
<sup>56</sup> Shandong University, Qingdao, Shandong, China
^{57} Seoul National University, Seoul, Republic of Korea
58 Sejong University, Seoul, Republic of Korea
<sup>59</sup> Shinshu University, Matsumoto, Nagano, Japan
60 Sungkyunkwan University, Suwon, Republic of Korea
61 Tel Aviv University, Tel Aviv, Israel
62 Tsinghua University, Beijing, China
63 Tsukuba University of Technology, Tsukuba, Ibaraki, Japan
64 University of Colorado Boulder, Boulder, CO, USA
65 University of Connecticut, Storrs, CT, USA
66 University of North Georgia, Dahlonega, GA, USA
```

⁶⁷ University of Houston, Houston, TX, USA

- 68 University of Illinois, Urbana, IL, USA
- 69 University of Kansas, Lawrence, KS, USA
- 70 University of Kentucky, Lexington, KY, USA
- 71 University of Ljubljana, Ljubljana, Slovenia
- 72 University of New Hampshire, Durham, NH, USA
- 73 University of Oslo, Oslo, Norway
- 74 University of Regina, Regina, SK, Canada
- ⁷⁵ University of Seoul, Seoul, Republic of Korea
- ⁷⁶ University of Tsukuba, Tsukuba, Japan
- ⁷⁷ University of Texas, Austin, TX, USA
- ⁷⁸ University of Tennessee, Knoxville, TN, USA
- ⁷⁹ University of Virginia, Charlottesville, VA, USA
- 80 Vanderbilt University, Nashville, TN, USA
- 81 Virginia Union University, Richmond, VA, USA
- 82 Wayne State University, Detroit, MI, USA
- 83 Weizmann Institute of Science, Rehovot, Israel
- 84 The College of William and Mary, Williamsburg, VA, USA
- ⁸⁵ Yamagata University, Yamagata, Japan
- 86 Yarmouk University, Irbid, Jordan
- 87 Yonsei University, Seoul, Republic of Korea
- 88 University of York, York, UK

ARTICLE INFO

Keywords: ECCE Electron Ion Collider Exclusive Near threshold Quarkonia

ABSTRACT

The EIC Comprehensive Chromodynamics Experiment (ECCE) detector has been recommended as a reference design for the proposed Electron-Ion Collider (EIC) program. This paper presents simulation studies of exclusive J/ψ detection and selected physics impact results in EIC using the projected ECCE detector concept. Exclusive quarkonium photoproduction is one of the most popular processes in EIC, which has a large cross section and a simple final state. Due to the gluonic nature of the exchange Pomeron, this process can be related to the gluon distributions in the nucleus. Preliminary results estimate the excellent statistics benefited from the large cross section of J/ψ photoproduction and superior performance of ECCE detector concept. The precise measurement of exclusive J/ψ photoproduction at EIC will help us to more deeply understand nuclear gluon distributions, near threshold production mechanism and nucleon mass structure.

1. Introduction

The future Electron-Ion Collider (EIC) is a novel, large-scale particle accelerator to be constructed at Brookhaven National Laboratory (BNL). The EIC science program reviewed by the National Academy of Sciences (NAS) [1] will address a broad set of fundamental questions. Probing the gluon density and understanding how quark and gluon interactions generate the nucleon mass are parts of key physics missions listed in NAS 2018 report [1]. In this article, we present a collection of physics impact studies related to exclusive J/ψ photoproduction based on theoretical projections and detector simulations.

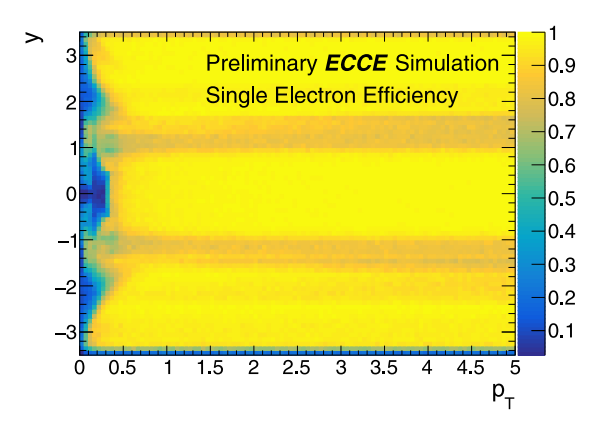
Nuclear parton distribution functions (nPDF) describe the behavior of bound partons in the nucleus. Most of the understanding of nPDF comes from fixed-target experiments. Determination of nPDF is through global fits to existing inclusive deep inelastic scattering (DIS) data. Constructing the ratio nPDF/PDF to quantified nuclear modifications is natural, which can cancel many of the theory uncertainties. A ratio below unity is called shadowing, while an enhancement is known as anti-shadowing. Recently a moderate gluon shadowing has been exhibited by J/ψ photoproduction data from LHC [2–4]. However, little is known about anti-shadowing at middle parton momentum fraction $x \sim 0.1$. The realization of the EIC with variable ion beam species will enable measurements of nPDF over a broad range of x and momentum transfer Q^2 . Photoproduction of vector meson via photon-Pomeron fusion is able to cleanly and clearly determine nuclear gluon PDFs at the EIC. With broad x coverage, J/ψ photoproduction can provide precise measurements to deepen our understanding of shadowing and anti-shadowing.

Exclusive photoproduction, which has a large cross section and a simple final state, is projected to play a prominent role in the quarkonia production processes at the EIC. In the reaction, a virtual incident photon fluctuates into a quark-antiquark pair, which scatters elastically off the target and emerges as a real quarkonium. The scattering process

occurs via the exchange of a color neutral object, Pomeron, which can be viewed as two gluons with self interaction (gluon ladder) in the language of QCD. Due to the gluonic nature of Pomeron, the exclusive quarkonia photoproduction at EIC can be related to the gluon distributions in the proton and nucleus using perturbative QCD. Furthermore, the distribution of momentum transfer from the target in the process is sensitive to the interaction sites, which provides a powerful tool to probe the spatial distribution of gluon in the nucleus.

Nucleons constitute about 99% of the mass of the visible universe. In the standard model, Higgs mechanism describes gauge bosons' "mass" generation. However it can only account for a small fraction of the nucleon mass. The major part comes from the strong interaction that binds quarks and gluons together. Understanding the hadron mass decomposition from strong interaction has become a topic of great interest in QCD. There are two key models [5-10] for the mass decomposition. One contains a trace anomaly contribution which is quantified by the energy-momentum tensor (EMT), and the other one agrees with an energy decomposition in the rest frame of the system. Recently, there has been sustained interest [11-13] among the nucleon structure community in determining the anomaly contribution M_a as a key to understanding the origin of the proton mass. Specifically, it has been proposed, based on some theorists' suggestions [14–16], that M_a can be accessed through the forward cross section via the exclusive production of quarkonia states such as J/ψ and Y. The trace anomaly is sensitive to the gluon condensate, with sensitivity greatest for production around the threshold. Even though it is argued that the trace anomaly is not an intrinsic part of the Hamiltonian, C'edric et al. stressed that measuring it remains an essential input for the precise estimate of the various contributions to a mass decomposition [17].

In this paper, we simulate exclusive J/ψ production using Fun4All framework with the designed ECCE detector system. In the simulation, we utilize eSTARLight model as the event generator for the exclusive photoproduction process. We make a projection of the exclusive J/ψ measurement at ECCE under the designed integrated luminosity of one year running for EIC to give an insight into related fruitful physics



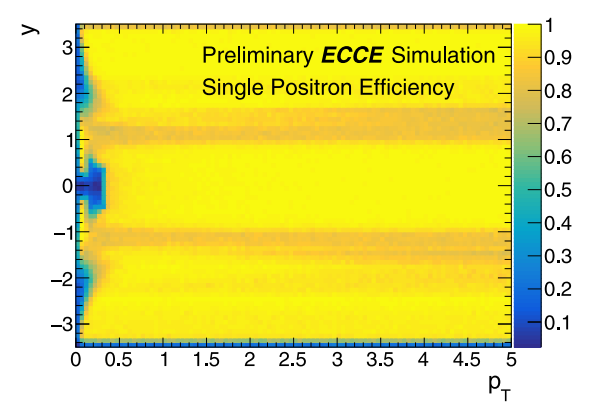


Fig. 1. Single track efficiency as a function of transverse momentum (p_T) and rapidity (y). Efficiency is calculated as the ratio of the number of reconstructed to generated J/ψ , so it is actually acceptance \times efficiency. Left Panel: e^- efficiency with the 1.4 T Babar magnet. Right Panel: e^+ efficiency.

opportunities, such as probing the nuclear gluon PDF, spatial distribution and proton mass decomposition. The major goal of this research is to present the detection capability and the physics opportunities which could be achieved with the ECCE detector setup for the exclusive process of ${\rm J}/\psi$ photoproduction.

2. Simulation framework of ECCE detector setup for J/ψ detection

The proposed ECCE detector has been designed and recommended as a reference detector concept following the U.S. Department of Energy's (DOE) Critical Decision 1 (CD-1) to accommodate the physics program for the EIC. The ECCE detector is a cylindrical detector covering $|\eta| \leq 3.5$ and the full azimuth. ECCE's tracking and vertexing systems use semiconductor and gaseous tracking detector technologies [18–20]: Monolithic Active Pixel Sensor (MAPS) based silicon vertex/tracking detector and μ Rwell based gas tracker derived from Gas Electron Multiplier (GEM) technology. According to the simulation of the designed tracking system, the momentum resolution of the central region and beam p-going direction is closed to or better than the requirement of Yellow Report (YR) [18]. More details regarding ECCE subsystems, performance and other selected physics objectives are provided in separate articles within the same issue [19–26].

For exclusive photoproduction of J/ψ , we adopt eSTARLight prediction of the cross section for $ep \rightarrow eJ/\psi p$ process with two minor improvements, detailed in Section 3. eSTARLight provides a photo-Pomeron interaction model parameterized by HERA data. In this study, two beam configurations, 5×41 GeV and 10×100 GeV, are used for e+p and e+Au collisions.

The detector response simulation is done by a GEANT4 based package called Fun4All. Four detector concepts have been developed and used in ECCE simulation and the latest January-Concept (2022) for the fourth simulation campaign is tagged with "Prop.7" software branch name [24]. In this work, the "Prop.7" detector concept is employed in J/ψ reconstruction via dielectron channel. Single e^+/e^- Tracking simulation results are shown as Fig. 1. The difference in efficiency between e^+ and e^- at very low p_T is due to the initial assumption parameter in the Kalman filter. If the beginning parameter is set to "positron", negative charge particles will have a low match quality and will likely be rejected.

The kinematic distribution of J/ψ for exclusive photoproduction is initialized by the theoretical calculation from eSTARLight. With this as input, we can obtain J/ψ reconstruction efficiency from the Fun4All package with ECCE detector setup seen in Fig. 2. The efficiency of J/ψ is almost independent of the rapidity and transverse momentum except for the edge area at large forward and backward rapidity. We also study the effect of magnetic field strength and bremsstrahlung energy loss of electron on J/ψ detection, shown as Figs. 3 and 4. At very low p_T (0.5 < p_T < 1.0 GeV/c), the improvement of the acceptance of the

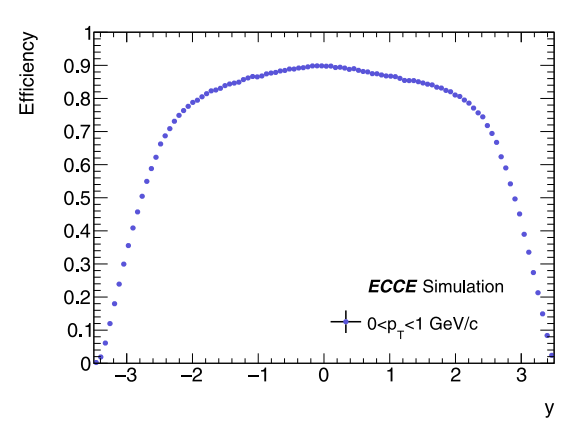


Fig. 2. Tracking efficiency of J/ψ as a function of rapidity from exclusive J/ψ simulation. "Efficiency" here is calculated as the ratio of the number of reconstructed to generated J/ψ , so it is actually acceptance × efficiency.

Table 1 Efficiency of mass window cut for J/ψ reconstruction to assess the magnitude of bremsstrahlung effect.

Mass window (GeV/c²)	Rapidity window		
	-3.5 < y < -1.5	-1.5 < y < 1.5	1.5 < y < 3.5
2.8-3.2	0.931	0.943	0.934
2.9-3.2	0.903	0.917	0.907
3.0-3.2	0.835	0.866	0.843

lower magnetic field strength accounts for the higher efficiency. While at larger p_T (1.0 < p_T < 2.0 GeV/c), there is no significant difference between efficiencies of 0.7 T and 1.4 T. The bremsstrahlung energy loss has already been put in tracking performance in the "Prop.7" concept detector, which constitutes the tail in the reconstructed mass distribution depicted as in Fig. 4. We scale the mass distribution to unity for the convenience of comparison, and the efficiencies of several mass window cuts are detailed in Table 1. As expected, the tail effect is more significant for the J/ψ at forward and backward rapidities (larger momentum of decayed electrons than that at central rapidity). With a proper mass cut window, the efficiency loss is minimal, implying that the effect of bremsstrahlung on J/ψ reconstruction with ECCE setup is not significant.

3. Theoretical setup for exclusive J/ψ production

This section presents the theoretical framework of exclusive J/ψ photoproduction in e+p and e+A collisions, which is employed in the simulation. The cross section of exclusive vector meson photoproduction $\sigma(eA \to eAV)$ is derived by integrating the photon flux caused

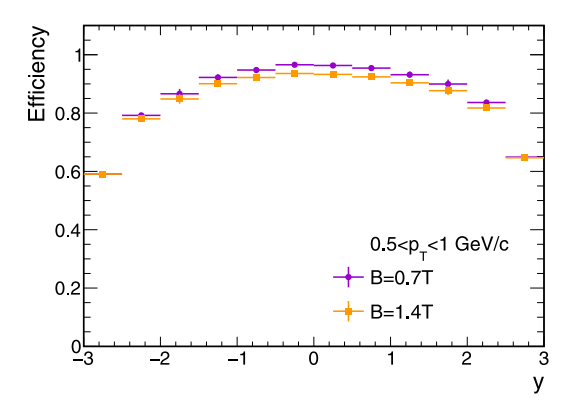


Fig. 3. Magnetic strength effect on efficiency as a function of rapidity at very low p_T (0.5 < p_T < 1.0 GeV/c).

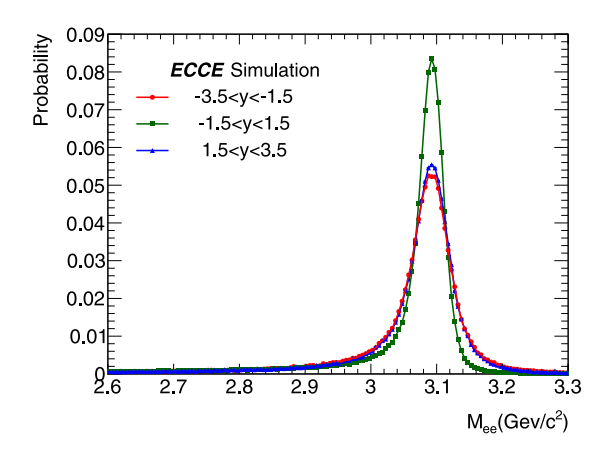


Fig. 4. Bremsstrahlung energy loss effect on J/ψ reconstruction. The bremsstrahlung effect on J/ψ reconstruction is displayed in three rapidity intervals for forward, central, backward regions.

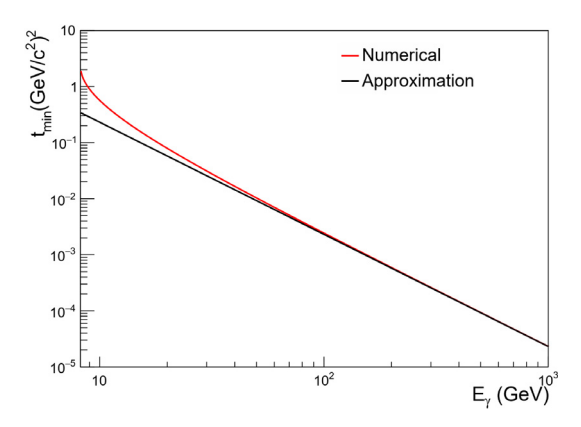


Fig. 5. The minimum momentum transfer (t_{min}) as a function of incident photon energy in the rest frame of the nuclear beam (target frame). Numerical line refers to true t_{min} used in this study from energy–momentum conservation of the process. Approximation line is the one used in eSTARLight.

by the electron beam and the virtual photon collision on the target nucleus, as illustrated in Eq. (1):

$$\sigma(eA \to eAV) = \int \frac{dW}{W} \int dk \int dQ^2 \frac{d^2 N_{\gamma}}{dk dQ^2} \sigma_{\gamma^* A \to VA} \left(W, Q^2 \right), \tag{1}$$

where the photon flux can be written as:

$$\frac{d^2 N_{\gamma}}{dk dQ^2} = \frac{\alpha}{\pi k Q^2} \left[1 - \frac{k}{Ee} + \frac{k^2}{2E_e^2} - \left(1 - \frac{k}{Ee} \right) \left| \frac{Q_{\min}^2}{Q^2} \right| \right]. \tag{2}$$

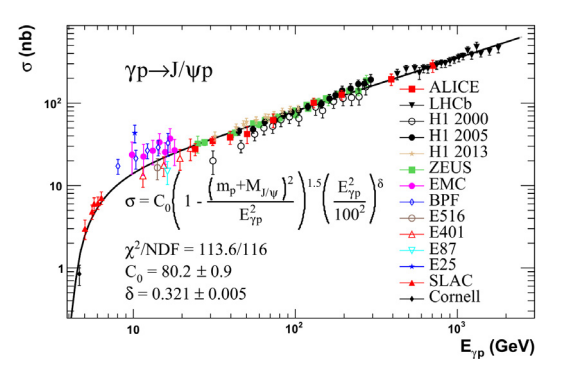


Fig. 6. The global fit of world-wide measurements of $\sigma(\gamma p \to V p)$ [27].

The cross section of virtual photon collision on the nucleus can be related to the production cross section with real photon:

$$\sigma_{\gamma^* A \to VA} (W, Q^2) = f(M_V) \sigma(W, Q^2 = 0) \left(\frac{M_V^2}{M_V^2 + Q^2}\right)^n$$

$$n = c_1 + c_2 (Q^2 + M_V^2),$$
(3)

where c_1 and c_2 are parameters determined by the HERA measurements. $f\left(M_V\right)$ is the Breit–Wigner distribution of the vector meson. And the cross section at $Q^2=0$ can be calculated by the integration of the forward scattering cross section and the square of the nucleus form factor, revealed as Eq. (4):

$$\sigma\left(W,Q^{2}=0\right)=\int_{t_{\min }}^{\infty }dt\frac{d\sigma(\gamma A\to VA)}{dt}\bigg|_{t=0}\left|F(t)\right|^{2},\tag{4}$$

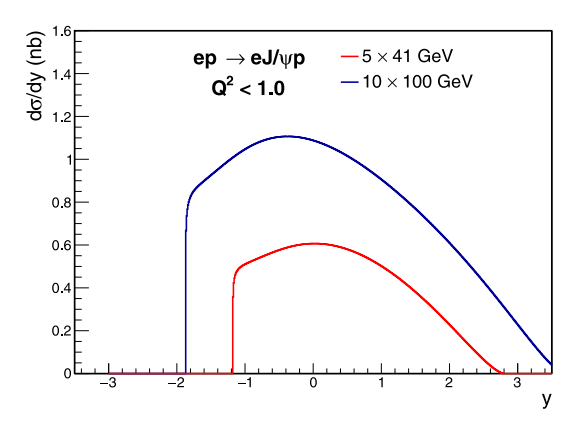
where $\frac{d\sigma(\gamma A \to VA)}{dt}|_{t=0}$ can be determined by $\frac{d\sigma(\gamma p \to Vp)}{dt}|_{t=0}$ via Glauber approach. The cross section of $\gamma p \to Vp$ can be parameterized using the world-wide measurements [27]. The framework is almost the same as eSTARLight [28,29], except for two minor improvements. At different center of photon–proton mass, the minimum momentum transfer squared t_{min} at the proton vertex could not always reach zero, so the low boundary of t is required in the integral of the cross section. In eSTARLight, t_{min} is approximated as $t_{min} = ((M_v)^2/2k)^2$. One can get the minimum of t when the transverse momentum of the produced vector meson is equal to zero. Then true t_{min} can be obtained from energy—momentum conservation of the $\gamma p \to Vp$ process in the target frame as Eqs. (5) and (6):

$$E_{\gamma} + m_p = \sqrt{M_v^2 + (E_{\gamma} - P_z^{\prime 2})} + \sqrt{m_p^2 + P_z^{\prime 2}},\tag{5}$$

$$t = (P' - P)^{2} = \left(\sqrt{m_{p}^{2} + P_{z}^{\prime 2}} - m_{p}\right)^{2} - P_{z}^{\prime 2},\tag{6}$$

where $P_z'^2$ is the longitudinal momentum of the final state proton. The photon energy dependence of t_{min} can be found in Fig. 5. The approximation in eSTARLight is proper at high photon energy. However, it would underestimate the magnitude at low values of photon energy, as is the case for our projection at ECCE. Furthermore, in eSTARLight, the parametrization of the $\gamma p \to V p$ cross section is only based on high-energy HERA data. The behavior of energy dependency is notably different between the high and low energy ranges, as demonstrated in Fig. 6, which would skew the computations at EIC. With these two improvements, the calculated results of rapidity distribution for exclusive J/ψ photoproduction in e+p and e+A collisions for 5×41 and 10×100 GeV collision energies are shown in Fig. 7. Q^2 dependence of e+p collision for 5×41 and 10×100 GeV with a rapidity range from -3 to 3 is illustrated in Fig. 8.

The raw counts per unit rapidity are shown in Fig. 9 for e+p and e+Au collisions for 10×100 GeV. For the projection results in the following section, we assume the integrated luminosity collected by ECCE is $100~fb^{-1}$ for e+p collisions and $10~fb^{-1}/A$ for e+Au collisions,



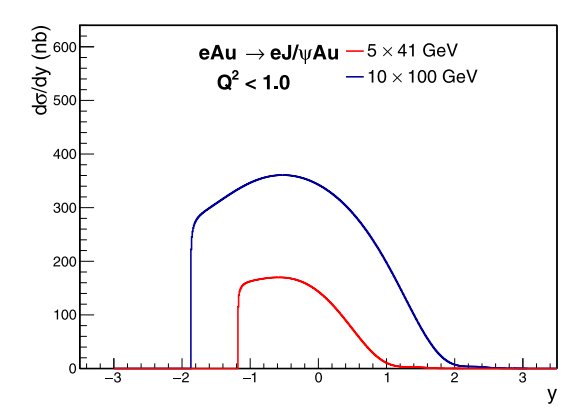


Fig. 7. Rapidity dependence of differential cross section of exclusive J/ψ photoproduction for $Q^2 < 1$ GeV². Projection are displayed with two beam configurations, e(5 GeV) × p(41 GeV) and e(10 GeV) × p(100 GeV).

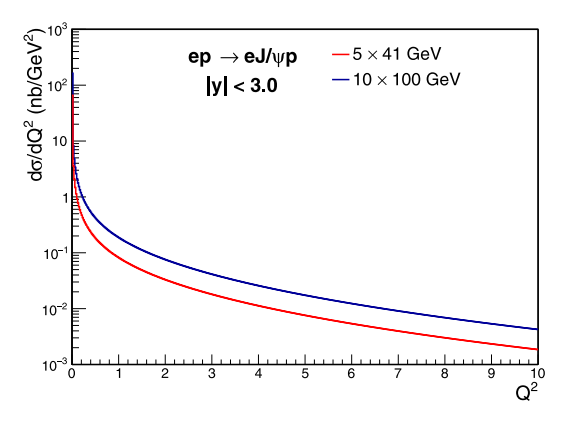


Fig. 8. The Q^2 dependence of differential cross section of exclusive J/ ψ photoproduction in e+p collision. Red and blue lines are for e(5 GeV) \times p(41 GeV) and e(10 GeV) \times p(100 GeV) collisions respectively.

where A is the mass number of Au. The figure shows that millions of $J/\psi s$ would be observed with the designed ECCE setup, which provides us with plenty of physics opportunities. And Q^2 dependence of the statistics of e+p collision in 5 × 41 and 10 × 100 GeV are shown in Fig. 10. As we can see, most events locate in the low Q^2 region, especially for $Q^2 < 1$ GeV².

4. Physics opportunities with exclusive J/ψ photoproduction at ECCE

4.1. Probe the nuclear gluon PDF

The gluon parton distribution functions (PDFs) in the proton and nucleus have large uncertainties because gluons do not carry any electric charge and cannot be directly determined by the DIS measurements. As mentioned in the introduction, the exclusive J/ψ photoproduction occurs via Pomeron exchange. Due to the gluonic nature of Pomeron, this process is directly sensitive to the gluon PDF. According to the calculation of perturbative QCD, the forward scattering cross section is proportional to the square of the gluon density distribution, shown in the following [30,31]:

$$\left. \frac{d\sigma(\gamma A \to V A)}{dt} \right|_{t=0} = \frac{\alpha_s^2 \Gamma_{ee}}{3\alpha M_V^{\xi}} 16\pi^3 \left[x g_A(x, \mu^2) \right]^2, \tag{7}$$

where Γ_{ee} is the width of the electronic decay of J/ψ , $g_A(x,\mu^2)$ is the gluon density and the momentum fraction x can be determined by the rapidity of J/ψ :

$$x = \frac{M_V e^y}{2E_N},\tag{8}$$

where E_N is the energy of nuclear beam per nucleon. Eq. (7) is derived from leading order (LO) pQCD calculation in the non-relativistic approximation [30], which indicates that the transverse momenta of c quarks in J/ψ are negligible. In that case, it is prescribed that $\mu^2 = M_V^2/4$.

The nuclear gluon shadowing can be model-independently quantified by R_{ν} :

$$R_{g} = \sqrt{\frac{\frac{d\sigma(\gamma A \to VA)}{dt}\Big|_{t=0}}{\frac{d\sigma(\gamma p \to Vp)}{dt}\Big|_{t=0}}}.$$
(9)

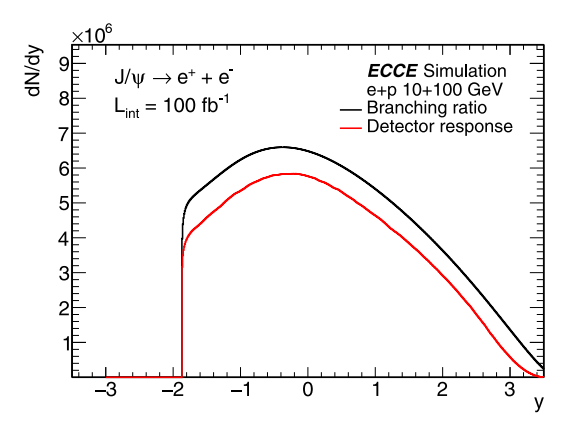
As shown in Eq. (7), if we make the forward scattering amplitude ratio between e+p and e+Au collisions, the shadowing factor R_g of gluon can be directly extracted. So measurements of J/ψ photoproduction can provide direct access to $g_A(x,\mu^2)$.

Elastic J/ ψ photoproduction processes are simulated in 10×100 (GeV) e+p and e+Au collisions with the framework described in the above sections. From the simulation, we extracted the $d^2\sigma/dtdy$ of J/ψ at t=0 for both e+p and e+Au collisions to make projection on R_{σ} . The uncertainty of the projection only includes the statistical error. At a given x, we can transfer it to the corresponding y value via Eq. (8) and get the statistics with the detector response. Then we fit the simulated t distribution with the predicted statistics and get the fit error of $d\sigma/dt$ for e+p and e+Au collisions at t = 0. The statistical error of projection can be extracted by the error propagation approach via R_{σ} equation in Eq. (8). As shown in Fig. 11, the measurement of exclusive J/ ψ production has a wide x coverage down to 2×10^{-3} for beam configuration 10×100 GeV. In the low x region, the EPPS16 [32] PDF set has a large uncertainty band, while the projected statistical error for ECCE is negligible. This shows that the precision exclusive J/ψ measurements at the EIC will significantly reduce the uncertainty of the nuclear gluon PDF at low values of x ($x < 10^{-2}$).

4.2. Probe the gluon spatial distribution

The Pomeron is the exchange object for the diffractive process, and diffraction is generally sensitive to spatial distribution. The momentum transfer from the target in the exclusive J/ψ photoproduction is sensitive to the production site, which provides us with a powerful tool to infer the spatial distribution of gluon in both proton and nucleus.

In the simulation, the Woods–Saxon distribution is used as input of the gluon source distribution F(b). We made a projection of t distribution for the processes in 10×100 (GeV) e+Au collisions with both coherent and incoherent J/ ψ photoproduction. The results are shown in Fig. 12, the red and blue curves are the coherent and incoherent contributions from calculations, respectively. The solid data points are the projected results from simulation, in which the statistical uncertainty is negligible. However, it should be noticed that according to the state



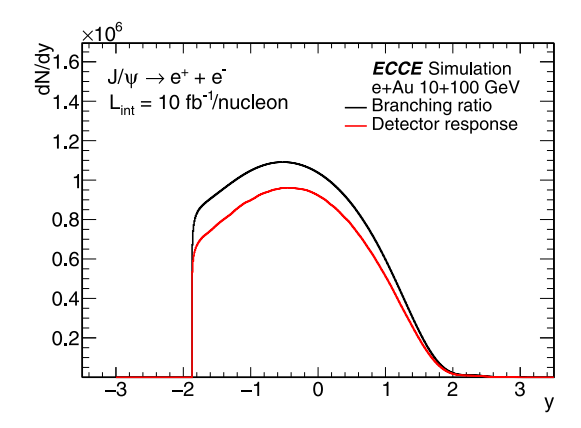
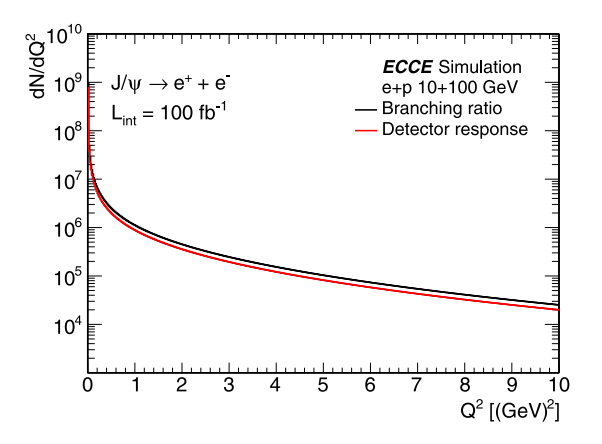


Fig. 9. Rapidity dependence statistics of coherent exclusive production of J/ψ in e+p and e+A collisions for 10×100 GeV. "Branching ratio" means taking the dielectron decay channel of J/ψ into account. "Detector response" refers to the yield considering detector efficiency modification. Left Panel: e+p collision. Right Panel: e+Au collision.



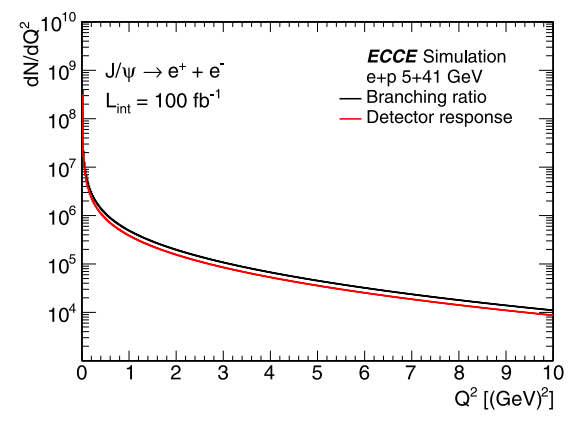


Fig. 10. The Q^2 dependence of J/ ψ photoproduction in e+p. "Branching ratio" means taking the dielectron decay channel of J/ ψ into account. "Detector response" refers to the yield considering detector efficiency modification. Left Panel: 10 × 100 GeV. Right Panel: 5 × 41 GeV.

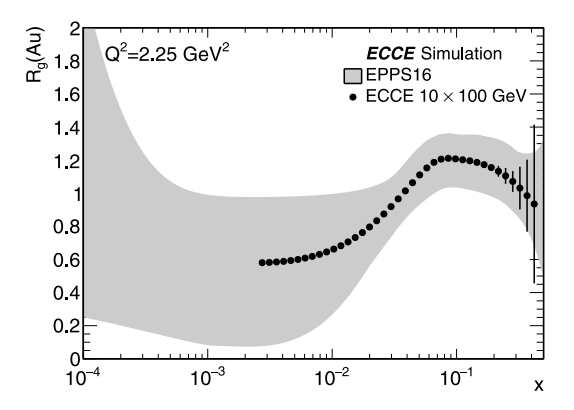


Fig. 11. Gluon nuclear shadowing factor as a function of momentum fraction x from 10×100 (GeV) e+Au collisions compared with uncertainty band of the gluon for Au at $Q^2 = 2.25$ GeV² for EPPS16.

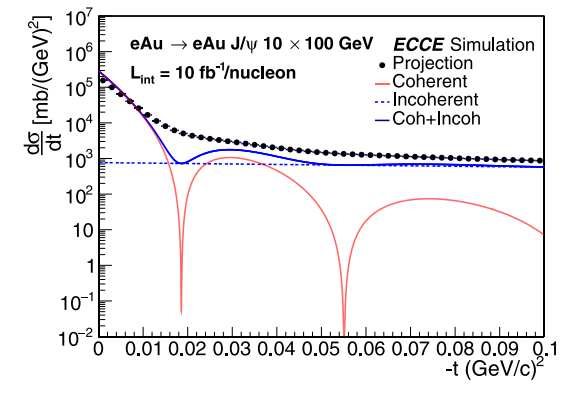


Fig. 12. t dependence of exclusive J/ψ production in 10 \times 100 (GeV) e+Au collision. Wood–Saxon distribution is used as input.

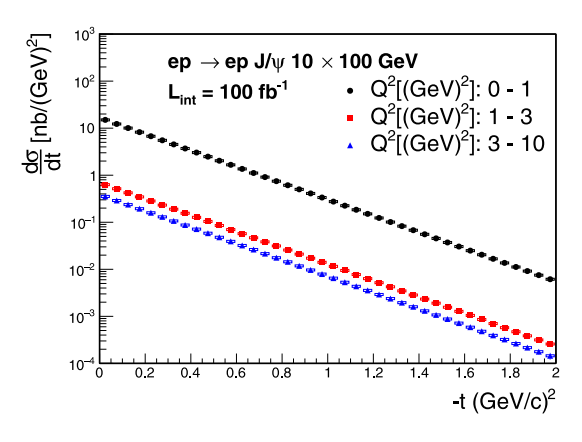
of the art theoretical calculation of elastic scattering, we will not get this minimum at these dips [33,34]. So the model here is a simplified and ideal one, and the purpose is to show the momentum resolution impact on this t dependence. Due to the momentum smearing from tracking system, the slope of the distribution is slightly different from that of theoretical calculations, and the diffraction dips are fold out. This suggests that the detector response should be precisely determined to extract the gluon spatial distribution.

The projected t distributions in 5×41 and 10×100 (GeV) e+p collisions are illustrated in Fig. 13 with the systematical and the statistical errors for different Q^2 regions (0–1, 1–3 and 3–10 GeV²). The statistical

error is determined with a similar approach given in Section 4.1. The systematical uncertainty is determined by the maximum deviation between the input and reconstructed t distribution. The statistical and systematical uncertainties are added in quadrature.

4.3. The near-threshold production mechanism

The elastic near-threshold J/ψ production can provide new insight into multi-quark, gluonic, hidden-color correlations of hadronic and nuclear wave-functions in QCD. Moreover, the measurements of this process probe the $x\sim 1$ configuration in the target, and the spectator



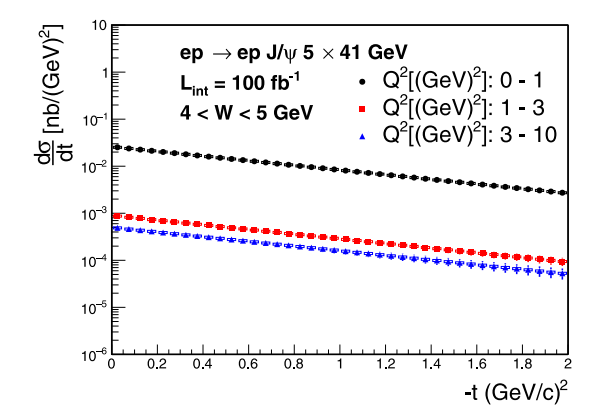


Fig. 13. t dependence of exclusive J/ψ production in 10×100 (GeV) e+p collision in several Q^2 intervals. Left Panel: 10×100 . Right Panel: 5×41 .

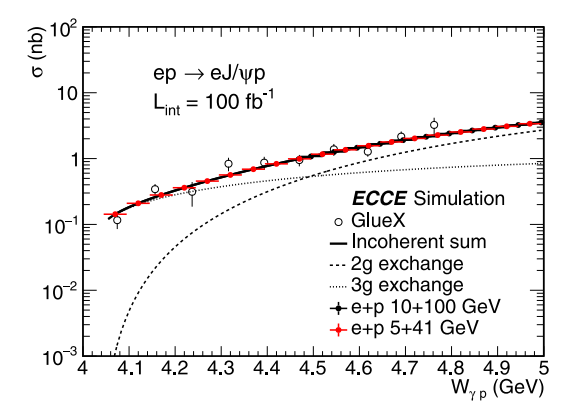


Fig. 14. Projection of J/ψ photoproduction cross section near threshold in 10×100 GeV and 5×41 GeV e+p collisions. 2+3 gluon exchange production model is employed to estimate the yield.

Fig. 15. Trace anomaly contribution as a function of γ p center of mass energy in 5+41 GeV e+p collisions. The integrated luminosity for e+p collisions is 100 fb^-1 .

partons carry a vanishing fraction $x \sim 0$ of the target momentum. This implies that the production rate behaves near $x \to 1$ as $(1 - x)^{2n_s}$, where n_s is the number of spectators. Then two gluon and three gluon exchange contributions can be written as [35]:

$$\frac{d\sigma}{dt} = \mathcal{N}_{2g} v \frac{(1-x)^2}{R^2 \mathcal{M}^2} F_{2g}^2(t) \left(W_{\gamma p}^2 - m_p^2 \right)^2, \tag{10}$$

$$\frac{d\sigma}{dt} = \mathcal{N}_{3g} v \frac{(1-x)^0}{R^4 \mathcal{M}^4} F_{3g}^2(t) \left(W_{\gamma p}^2 - m_p^2\right)^2, \tag{11}$$

where *R* is the radius of proton, *M* is the mass of J/ψ , and $W_{\gamma p}$ is the center of mass energy of γp .

The projected results for near-threshold production for 10×100 GeV and 5×41 GeV e+p collisions are shown in Fig. 14. The GlueX results, two and three gluon exchange contributions are also shown for comparison. All the theoretical curves and projection results are normalized with the GlueX measurements. The error bars on GlueX measurements represent only statistical uncertainties. At low $W_{\gamma p} < 4.5$ GeV region, the cross section is dominated by three gluon exchange process. At $W_{\gamma p} > 4.5$ GeV, two gluon exchange process comes to take control. For 10 × 100 GeV e+p collisions, the center-of-mass energy can only reach as low as 4.5 GeV due to the limited detector coverage. But for 5 × 41 GeV e+p collisions, they cover the whole near-threshold range. The GlueX experiment at JLab has already shed light on the nearthreshold production mechanism as a sum of two-gluon and three-gluon exchange and set limits on pentaquark production [36]. Measurements of near-threshold with larger statistics and broader $W_{\nu p}$ range at the EIC has the potential to impose more powerful constraints on the production mechanism, like charmed pentaquark P_c production [37, 38].

4.4. Trace anomaly and proton mass decomposition

According to QCD theory, there are four terms of decomposition in nucleon mass as Eq. (12) [39]: quark energy M_q , gluon energy M_g , quark mass M_m and the trace anomaly contribution M_a , and these terms are sensitive to the momentum fraction a carried by all quarks and the trace anomaly parameter b.

$$M_{q} = \frac{3}{4} \left(a - \frac{b}{1 + \gamma_{m}} \right) M_{N},$$

$$M_{g} = \frac{3}{4} (1 - a) M_{N},$$

$$M_{m} = \frac{4 + \gamma_{m}}{4 \left(1 + \gamma_{m} \right)} b M_{N},$$

$$M_{a} = \frac{1}{4} (1 - b) M_{N},$$
(12)

Recent theoretical efforts from VMD model and Holographic model [40–42] suggest that the trace anomaly parameter can be extracted by the near-threshold exclusive quarkonia process via their production at $(d\sigma/dt)|_{t=t_{min}}$. In the simulation, we made the projection of the trace anomaly parameter restriction capability at ECCE. The results are shown in Figs. 15 and 16, which can provide precise information on the nucleon mass decomposition. The GlueX result [39] of the trace anomaly is also shown for comparison. The projection uncertainty consists of two parts, the statistical error using similar method as Section 4.1 and systematical error defined in Section 4.2. The $d\sigma/dt|_{t=0}$ can be related to the trace anomaly parameter with Eqs. (13), (14),

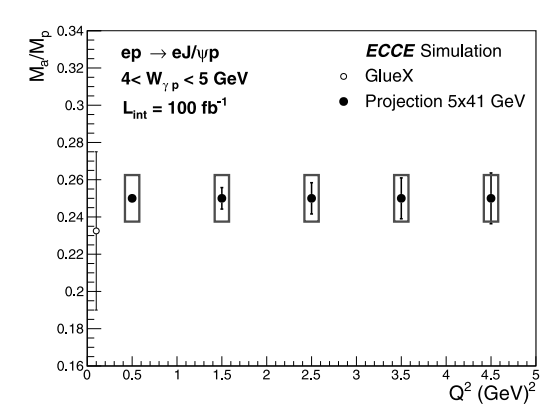


Fig. 16. Trace anomaly contribution as a function of Q^2 in 5+41 GeV e+p collisions. The integrated luminosity for e+p collisions is 100 fb^-1 .

(15) [39],

$$\left. \frac{d\sigma_{\gamma N \to J/\psi N}}{dt} \right|_{t=0} = \left. \frac{3\Gamma \left(J/\psi \to e^+ e^- \right)}{\alpha m_{J/\psi}} \left(\frac{k_{J/\psi N}}{k_{\gamma N}} \right)^2 \frac{d\sigma_{J/\psi N \to J/\psi N}}{dt} \right|_{t=0}, \tag{13}$$

$$\left. \frac{d\sigma_{J/\psi N \to J/\psi N}}{dt} \right|_{t=0} = \frac{1}{64\pi} \frac{1}{m_{J/\psi}^2 \left(\lambda^2 - m_N^2\right)} \left| F_{J/\psi N} \right|^2, \tag{14}$$

where $k_{ab}^2 = \left[s - \left(m_a + m_b\right)^2\right] \left[s - \left(m_a - m_b\right)^2\right]/4s$ denotes the squared momentum of center-of-mass of the corresponding two-body system, Γ is the decay width of specific channel, α is the fine structure constant. $\lambda = \left(p_N p_{J/\psi}/m_{J/\psi}\right)$ is the energy of nucleon in the J/ψ rest frame. At low energy, the forward amplitude $F_{J/\psi N}$ can be approximately written as a function of (1-b) in Eq. (15), and the relative uncertainty of $d\sigma/dt|_{t=0}$ can be used to get the uncertainty of M_a/M_p (\propto (1-b)) via the error propagation formula.

$$F_{J/\psi N} \simeq r_0^3 d_2 \frac{2\pi^2}{27} \left(2M_N^2 - \left\langle N \left| \sum_{i=u,d,s} m_i \bar{q}_i q_i \right| N \right\rangle \right)$$

$$\simeq r_0^3 d_2 \frac{2\pi^2}{27} \left(2M_N^2 - 2bM_N^2 \right)$$

$$\simeq r_0^3 d_2 \frac{2\pi^2}{27} 2M_N^2 (1-b),$$
(15)

where r_0 is the "Bohr" radius of J/ψ , and d_2 is the Wilson coefficient. These two parameters can be treated as constant in the relationship between $d\sigma/dt|_{t=0}$ and (1-b) at low energy, thus could be neglected in the uncertainty determination.

5. Summary

In this paper, we simulate exclusive J/ψ production using Fun4All framework with the designed ECCE detector system at the future EIC. For J/ψ detection, ECCE has good reconstruction efficiency and broad coverage, with large statistics for the designed EIC luminosity. We also demonstrate the capability of ECCE to probe the related physics opportunities for the exclusive J/ψ photoproduction process. For gluon distribution in the proton and nucleus, the projection of the gluon nuclear shadowing effect shows an excellent capability of constraining the nuclear gluon PDF with the exclusive J/ψ forward scattering measurements at ECCE. Benefited from the unprecedented coverage and excellent reconstruction capability, ECCE can provide a strong constraint to the near-threshold production mechanism of the exclusive J/ψ photoproduction process. Furthermore, the projection results of the near-threshold exclusive quarkonia production also show an excellent capability to extract the trace anomaly parameter to precisely determine the nucleon mass decomposition.

Declaration of competing interest

The authors declare that they have no known competing financial interests or personal relationships that could have appeared to influence the work reported in this paper.

Acknowledgments

X. Li and W. Zha are supported by the National Natural Science Foundation of China (12005220, 12175223) and MOST (2018YFE0104900). The authors would like to thank the ECCE Consortium for performing a full simulation of their detector design, for providing up-to-date information on EIC run conditions, and for suggestions and comments on the manuscript. X. Li and W. Zha would like to thank Y. Zhou for useful suggestions and discussions related to this analysis.

W. Zha is supported by Anhui Provincial Natural Science Foundation No. 2208085J23 and Youth Innovation Promotion Association of Chinese Academy of Sciences.

AANL group are supported by the Science Committee of RA, in the frames of the research project N 21AG-1C028.

References

- [1] National Academies of Sciences Engineering and Medicine, An Assessment of U.S.-Based Electron-Ion Collider Science, The National Academies Press, Washington, DC, 2018, http://dx.doi.org/10.17226/25171, URL https://nap.nationalacademies.org/catalog/25171/an-assessment-of-us-based-electron-ion-collider-science.
- [2] B. Abelev, et al., Coherent J/ ψ photoproduction in ultra-peripheral Pb–Pb collisions at $s_{NN}=2.76$ TeV, Phys. Lett. B 718 (4) (2013) 1273–1283, http://dx. doi.org/10.1016/j.physletb.2012.11.059, URL https://www.sciencedirect.com/science/article/pii/S0370269312012257.
- [3] V. Khachatryan, et al., Coherent J/ψ photoproduction in ultra-peripheral Pb-Pb collisions at s_{NN} = 2.76 TeV with the CMS experiment, Phys. Lett. B 772 (2017) 489–511, http://dx.doi.org/10.1016/j.physletb.2017.07.001, URL https://www.sciencedirect.com/science/article/pii/S0370269317305488.
- [4] E. Abbas, et al., Charmonium and e^+e^- pair photoproduction at mid-rapidity in ultra-peripheral Pb-Pb collisions at $s_{NN}=2.76$ TeV, Eur. Phys. J. C 73 (11) (2013) http://dx.doi.org/10.1140/epjc/s10052-013-2617-1, URL https://link.springer.com/article/10.1140/epjc/s10052-013-2617-1.
- [5] X. Ji, QCD analysis of the mass structure of the nucleon, Phys. Rev. Lett. 74 (7) (1995) 1071–1074, http://dx.doi.org/10.1103/physrevlett.74.1071, URL http://dx.doi.org/10.1103/PhysRevLett.74.1071.
- [6] C. Lorcé, On the hadron mass decomposition, Eur. Phys. J. C 78 (120) (2018) http://dx.doi.org/10.1140/epjc/s10052-018-5561-2, URL http://dx.doi.org/10. 1140/epjc/s10052-018-5561-2.
- A. Metz, B. Pasquini, S. Rodini, Revisiting the proton mass decomposition, Phys. Rev. D 102 (11) (2020) http://dx.doi.org/10.1103/physrevd.102.114042, URL http://dx.doi.org/10.1103/PhysRevD.102.114042.
- [8] C. Roberts, Empirical consequences of emergent mass, Symmetry 12 (9) (2020) 1468, http://dx.doi.org/10.3390/sym12091468, URL http://dx.doi.org/10.3390/sym12091468.
- [9] K. Tanaka, Three-loop formula for quark and gluon contributions to the QCD trace anomaly, J. High Energy Phys. 2019 (1) (2019) http://dx.doi.org/10.1007/jhep01(2019)120, URL http://dx.doi.org/10.1007/JHEP01(2019)120.
- [10] M. Shifman, A. Vainshtein, V. Zakharov, Remarks on higgs-boson interactions with nucleons, Phys. Lett. B 78 (4) (1978) 443–446, http://dx.doi.org/10.1016/ 0370-2693(78)90481-1, URL https://www.sciencedirect.com/science/article/pii/ 0370269378904811.
- [11] X. Ji, Breakup of hadron masses and energy-momentum tensor of QCD, Phys. Rev. D 52 (1995) 271–281, http://dx.doi.org/10.1103/PhysRevD.52.271, arXiv: hep-ph/9502213
- [12] X. Ji, Proton mass decomposition: naturalness and interpretations, Front. Phys. (Beijing) 16 (6) (2021) 64601, http://dx.doi.org/10.1007/s11467-021-1065-x, arXiv:2102.07830.
- [13] Y. Guo, X. Ji, Y. Liu, QCD analysis of near-threshold photon-proton production of heavy quarkonium, Phys. Rev. D 103 (9) (2021) 096010, http://dx.doi.org/ 10.1103/PhysRevD.103.096010, arXiv:2103.11506.
- [14] S. Brodsky, E. Chudakov, P. Hoyer, J. Laget, Photoproduction of charm near threshold, Phys. Lett. B 498 (1–2) (2001) 23–28, http://dx.doi.org/10. 1016/s0370-2693(00)01373-3, URL http://dx.doi.org/10.1016/S0370-2693(00) 01373-3.

- [15] O. Gryniuk, M. Vanderhaeghen, Accessing the real part of the forward J/ψ-p scattering amplitude from J/ψ Photoproduction on protons around threshold, Phys. Rev. D 94 (7) (2016) http://dx.doi.org/10.1103/physrevd.94.074001, URL http://dx.doi.org/10.1103/PhysRevD.94.074001.
- [16] M. Du, V. Baru, F. Guo, C. Hanhart, U.-G. Meißner, A. Nefediev, I. Strakovsky, Deciphering the mechanism of Near-Threshold J/ψ Photoproduction, Eur. Phys. J. C 80 (11) (2020) http://dx.doi.org/10.1140/epjc/s10052-020-08620-5, URL http://dx.doi.org/10.1140/epjc/s10052-020-08620-5.
- [17] C. Lorcé, A. Metz, B. Pasquini, S. Rodini, Energy-momentum tensor in QCD: nucleon mass decomposition and mechanical equilibrium, J. High Energy Phys. 2021 (11) (2021) http://dx.doi.org/10.1007/jhep11(2021)121.
- [18] R. Abdul Khalek, et al., Science requirements and detector concepts for the electron-ion collider: EIC vellow report, 2021, arXiv:2103.05419.
- [19] First Authors, et al., ECCE Consortium Collaboration, Design of the ECCE detector for the electron ion collider, Nucl. Instrum. Methods A (2022) in this issue, https: //doi.org/10.48550/ARXIV.2209.02580, URL https://arxiv.org/abs/2209.02580.
- [20] X. Li, et al., ECCE Consortium Collaboration, Open heavy flavor studies for the ECCE detector at the electron ion collider, Nucl. Instrum. Methods A (2022) in this issue, https://doi.org/10.48550/ARXIV.2207.10632, URL https://arxiv.org/ abs/2207.10632.
- [21] First Authors, et al., ECCE Consortium Collaboration, Design and simulated performance of calorimetry systems for the ECCE detector at the electron ion collider, Nucl. Instrum. Methods A (2022) in this issue.
- [22] First Authors, et al., ECCE Consortium Collaboration, Design and simulated performance of tracking systems for the ECCE detector at the electron ion collider, Nucl. Instrum. Methods A (2022) in this issue.
- [23] First Authors, et al., ECCE Consortium Collaboration, eA diffractive production with the ECCE detector at the electron ion collider, Nucl. Instrum. Methods A (2022) in this issue.
- [24] First Authors, et al., ECCE Consortium Collaboration, Exclusive and diffractive processes and tagging with the ECCE detector at the electron ion collider, Nucl. Instrum. Methods A (2022) in this issue.
- [25] First Authors, et al., ECCE Consortium Collaboration, Deep learning-based lepton identification for the ECCE detector, Nucl. Instrum. Methods A (2022) in this issue
- [26] First Authors, et al., ECCE Consortium Collaboration, AI-assisted optimization of the ECCE tracking system, Nucl. Instrum. Methods A (2022) in this issue.
- [27] Z. Cao, L. Ruan, Z. Tang, Z. Xu, C. Yang, S. Yang, W. Zha, Photoproduction of J/ψ in non-single-diffractive p+p collisions, Chin. Phys. C 43 (6) (2019) 064103, http://dx.doi.org/10.1088/1674-1137/43/6/064103.
- [28] M. Lomnitz, S. Klein, Exclusive vector meson production at an electron-ion collider, Phys. Rev. C 99 (2019) 015203, http://dx.doi.org/10.1103/PhysRevC. 99.015203, URL https://link.aps.org/doi/10.1103/PhysRevC.99.015203.
- [29] W. Zha, S.R. Klein, R. Ma, L. Ruan, T. Todoroki, Z. Tang, Z. Xu, C. Yang, Q. Yang, S. Yang, Coherent J/ψ Photoproduction in hadronic heavy-ion collisions, Phys. Rev. C 97 (2018) 044910, http://dx.doi.org/10.1103/PhysRevC.97.044910, URL https://link.aps.org/doi/10.1103/PhysRevC.97.044910.
- [30] V. Guzey, M. Zhalov, Exclusive J/ψ production in ultraperipheral collisions at the LHC: constraints on the gluon distributions in the proton and nuclei, J. High Energy Phys. 2013 (10) (2013) http://dx.doi.org/10.1007/jhep10(2013) 207. URL http://dx.doi.org/10.1007/JHEP10(2013)207.

- [31] V. Guzey, M. Zhalov, Rapidity and momentum transfer distributions of coherent J/ψ Photoproduction in ultraperipheral ppb collisions at the LHC, J. High Energy Phys. 2014 (2) (2014) http://dx.doi.org/10.1007/jhep02(2014)046, URL http://dx.doi.org/10.1007/JHEP02(2014)046.
- [32] K.J. Eskola, P. Paakkinen, H. Paukkunen, C.A. Salgado, EPPS16: nuclear parton distributions with LHC data, Eur. Phys. J. C 77 (3) (2017) http://dx.doi.org/ 10.1140/epjc/s10052-017-4725-9, URL http://dx.doi.org/10.1140/epjc/s10052-017-4725-9
- [33] X. Roca-Maza, M. Centelles, F. Salvat, X. Viñas, Theoretical study of elastic electron scattering off stable and exotic nuclei, Phys. Rev. C 78 (2008) 044332, http://dx.doi.org/10.1103/PhysRevC.78.044332, URL https://link.aps.org/doi/10.1103/PhysRevC.78.044332.
- [34] J. Liu, R. Xu, J. Zhang, C. Xu, Z. Ren, Elastic electron scattering off nuclei with shape coexistence, J. Phys. G: Nucl. Part. Phys. 46 (5) (2019) 055105, http://dx.doi.org/10.1088/1361-6471/ab029a.
- [35] S. Brodsky, E. Chudakov, P. Hoyer, J. Laget, Photoproduction of charm near threshold, Phys. Lett. B 498 (1-2) (2001) 23-28, http://dx.doi.org/10. 1016/s0370-2693(00)01373-3, URL http://dx.doi.org/10.1016/s0370-2693(00) 01373-3.
- [36] A. Ali, et al., GlueX Collaboration, First measurement of near-threshold Jψ exclusive photoproduction off the proton, Phys. Rev. Lett. 123 (2019) 072001, http://dx.doi.org/10.1103/PhysRevLett.123.072001, URL https://link.aps.org/doi/10.1103/PhysRevLett.123.072001.
- [37] Q. Wang, X. Liu, Q. Zhao, Photoproduction of hidden charm pentaquark states P_c⁺(4380) and P_c⁺(4450), Phys. Rev. D 92 (2015) 034022, http://dx.doi.org/10. 1103/PhysRevD.92.034022, URL https://link.aps.org/doi/10.1103/PhysRevD.92. 034022
- [38] A.N.H. Blin, C. Fernández-Ramírez, A. Jackura, V. Mathieu, V.I. Mokeev, A. Pilloni, A.P. Szczepaniak, Joint Physics Analysis Center Collaboration, Studying the P_c(4450) resonance in J/ψ photoproduction off protons, Phys. Rev. D 94 (2016) 034002, http://dx.doi.org/10.1103/PhysRevD.94.034002, URL https://link.aps.org/doi/10.1103/PhysRevD.94.034002.
- [39] R. Wang, X. Chen, J. Evslin, The origin of proton mass from J/ψ photoproduction data, Eur. Phys. J. C 80 (6) (2020) 507, http://dx.doi.org/10.1140/epic/s10052-020-8057-9.
- [40] K.A. Mamo, I. Zahed, Diffractive Photoproduction of J/ψ and Y using holographic QCD: Gravitational form factors and GPD of gluons in the proton, Phys. Rev. D 101 (2020) 086003, http://dx.doi.org/10.1103/PhysRevD.101.086003, URL https://link.aps.org/doi/10.1103/PhysRevD.101.086003.
- [41] Y. Hatta, D. Yang, Holographic J/ψ production near threshold and the proton mass problem, Phys. Rev. D 98 (2018) 074003, http://dx.doi.org/10.1103/PhysRevD.98.074003, URL https://link.aps.org/doi/10.1103/PhysRevD.98.074003.
- [42] R. Boussarie, Y. Hatta, QCD analysis of Near-Threshold quarkonium leptoproduction at large photon virtualities, Phys. Rev. D 101 (11) (2020) http://dx.doi.org/10.1103/physrevd.101.114004, URL http://dx.doi.org/10.1103/PhysRevD.101.114004.